Nuclear Materials and Energy 000 (2016) 1–6

Contents lists available at ScienceDirect

Nuclear Materials and Energy

journal homepage: www.elsevier.com/locate/nme

Fe^+ ion irradiation induced changes in structural and magnetic properties of iron films

K. Papamihail[a,b], K. Mergia[a,*], F. Ott[c], Yves Serruys[d], Th. Speliotis[a], G. Apostolopoulos[a], S. Messoloras[a]

[a] Fusion Technology Group, National Center for Scientific Research "Demokritos", 15310 Athens, Greece
[b] Solid State Physics Department, Faculty of Physics, National and Kapodistrian University of Athens, 15784 Zografou, Greece
[c] Laboratoire Léon Brillouin CEA/CNRS, CEA Saclay, 91191 Gif sur Yvette Cedex, France
[d] Laboratoire JANNUS DEN/DMN/SRMP, CEA Saclay, 91191 Gif sur Yvette Cedex, France

ARTICLE INFO

Article history:
Received 16 November 2015
Revised 24 February 2016
Accepted 11 March 2016
Available online xxx

Keywords:
Ion irradiation
Implantation
Iron
Magnetism
Polarized neutron reflectivity
Grain size

ABSTRACT

490 keV Fe^+ ion irradiation of 200 nm thick Fe films was found to induce both structural and magnetic changes. Both, the lattice constant and the grain size increase as a function of dose and both properties follow the same power law. Irradiation induces a depth dependent magnetic profile consisting of two sublayers. The top Fe sublayer has a magnetic moment higher than that of the Fe before the irradiation whereas the bottom sublayer lower. The two sublayers are connected with the effects of Fe^+ irradiation, i.e. the top sublayer with the depth in which mainly radiation damage occurs whereas the bottom one with the implantation of impinging Fe^+ ions. The magnetic moments of the two sublayers have a non-monotonous variation with irradiation dose depicting a maximum for the top sublayer and a minimum for the bottom one at 96.2 dpa ('displacements per atom'). The magnetic moment enhancement/reduction is discussed in relation with the atomic volume variation in the case of atom displacements and/or implantation effects.

1. Introduction

Although significant progress has been made in the development of improved radiation resistant alloys, the so far developed alloys are unable to withstand the severe operational conditions expected in fusion power plants [1–3]. Therefore, there is need for developing new radiation resistant alloys and to that end there is an international effort aspiring into understanding the effects of neutron radiation damage. In order to materialize this objective multiscale modeling, experimental validation and irradiation campaigns in fission reactors [4,5] are implemented. The last activity suffers from a vital inadequacy concerning fusion applications as the validity of extrapolating the fission neutron irradiation results to fusion environment is questionable. This contention arises from the fact that the energy spectrum of fission neutrons (mean energy of about 2 MeV) within a material is very different to that produced from the 14 MeV fusion neutrons. This shortcoming of the experimental basis of the research on neutron radiation damage to be generated in a fusion reactor can be surmounted by appreciating that the dominant damage arises from Primary Knock-on Atoms (PKA). Therefore, the main features of the neutron induced radiation damage in the materials can be studied by employing self-ion irradiations [6]. As the energy of the impinging ions is well determined averaging effects of different PKA energies can be avoided and also a wide choice of ion energies and fluxes are available for a methodical study of the damage. Implementation of ion irradiation has the additional advantage that the radiation damage arising solely from PKA can be studied by avoiding neutron transmutations e.g. helium and hydrogen production. Further, the ion irradiated samples are not radio-active and they can be examined immediately after irradiations employing all the available material science techniques. Therefore, the experimental results on the damage produced by energetic ions provide significant and comprehensible information on radiation damage and they consist a rewarding testing bed for theoretical models and simulations. It is worth mentioning that the cost of ion irradiation in accelerators is very low in comparison to neutron irradiations in fission reactors.

It was chosen to utilize the above expressed viewpoint on Fe as ferritic/martensitic FeCr based steels are candidate structural materials for the future fusion reactor. The energy of the Fe ions for

* Corresponding author. Tel.: +302106503706.
E-mail address: kmergia@ipta.demokritos.gr (K. Mergia).

http://dx.doi.org/10.1016/j.nme.2016.03.006

the irradiations was defined to 490 keV as this is the mean energy of the Fe PKA produced by the 14 MeV fusion neutrons impinging on iron based alloys. As the range of this energy ions is of the order of few hundreds of nanometers samples in the form of films have to be employed. Thus, films of 200 nm thickness were employed in order to observe effects arising from both radiation damage and ion implantation. The current works refers to the effect of Fe^+ ion irradiation on the structural and magnetic properties of the 200 nm thick iron films whereas in a previous work [7] 60 nm thick Fe films, in which only radiation damage occurs, were investigated. Irradiations with 490 keV Fe^+ ion beam were performed for different doses. The structural characterization of the samples before and after the irradiations was performed using grazing and normal incidence X-ray diffraction and X-ray reflectivity measurements. The induced magnetic state changes were determined by magnetic hysteresis loop and polarized neutron reflectivity measurements. Magnetic hysteresis loop measurements refer to the magnetic properties of the total film thickness, whereas by polarized neutron reflectivity (PNR) the magnetic moment per atom versus depth is determined.

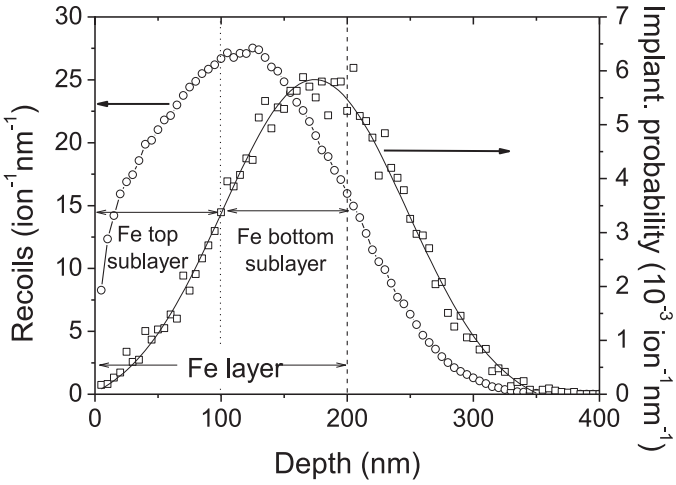

Fig. 1. Recoils and implantation profile for 490 keV Fe^+ on Fe target according to SRIM calculations. For the definition of top and bottom Fe sublayer refer to Fig. 8a.

2. Materials and methods

Iron films having a thickness of 200 nm were fabricated on one side polished (001) silicon wafer substrates using DC magnetron sputtering. A Cr cover layer of 4 nm nominal thickness was deposited on top of the Fe layer in order to prevent oxidization.

Irradiations with 490 keV Fe^+ ion beam were performed at JANNuS facility at CEA-Saclay using an ion flux of around 2×10^{12} ions/(cm^2 s). The samples during the irradiation were placed on a liquid nitrogen cooled flange compensating the heating induced by the beam and thus keeping the sample temperature at 25 °C. The damage is characterized in terms of the average number of times that an individual atom is displaced from its lattice site i.e. 'displacements per atom' (dpa) and this unit is employed throughout this paper. The samples were irradiated for different doses which correspond to a range from 0.5 to 341 dpa (Table 1).

Simulations using the SRIM-2008 software [8] have been performed of the bombardment of 490 keV Fe^+ ions on an iron target using for the displacement energy the value of 40 eV [ASTM standard, 9]. In Fig. 1 are depicted the number of recoils and the ion implantation probability per incident ion versus the depth within the iron target. It is observed that up to a depth of around 100 nm mainly radiation damage occurs and above 100 nm up both radiation and implantation effects take place.

The films were characterized before and after the irradiation for both the structural and magnetic properties. The structural characterization was carried out by X-ray reflectivity (XRR) and X-ray diffraction (XRD) both at normal and grazing incidence angle. The X-ray measurements were performed on a D8 Advance Bruker diffractometer using Cu-Kα radiation and a parallel beam stemming from a Göbel Mirror. The magnetic state of the samples was determined by Vibrating Sample Magnetometry and Polarized Neutron Reflectivity (PNR) measurements. The PNR measurements were performed at PRISM instrument at Laboratoire Léon-Brillouin, CEA-Saclay. An in-plane external magnetic field of 1.2 T was applied in order to magnetically saturate the samples. The incident neutron wavelength was 0.40 nm and the Q-range varied from 0.05 to 2.3 nm^{-1} (Q is the magnitude of scattering vector, $\boldsymbol{Q} = \boldsymbol{k'} - \boldsymbol{k}$, where $\boldsymbol{k'}$ and $\boldsymbol{k}$ the wave vector of the scattered and incident beam, respectively). In PNR measurements we obtain two reflectivities the one, R^+, corresponding to the spin of incident neutron being parallel to the applied magnetic field (spin up) and the second, R^-, to the spin being down. The spin up and down reflectivities can be calculated from the exact solution of the Schrödinger equation for an assumed model of density and magnetic moment profile versus depth. The parameters characterizing the density model (e.g. thickness, density, magnetic moment per atom) are derived by a least squares fit to the experimental data using the SimulReflec software [10].

Table 1
Irradiation parameters.

Ion flux ($\times 10^{12}$ ions/(cm^2 s))	Irradiation time (min)	Dose ($\times 10^{15}$ ions/cm^2)	Dose (dpa)
2.4	1.5	0.2	0.5
	2.5	0.4	1.1
	29	3.6	9.2
	93	10.8	27.6
	308	37.9	96.2
	984	134.1	341

3. Results

3.1. Structural changes induced by the Fe^+ irradiations

Initially any structural changes induced by the Fe^+ ion irradiation of the Fe films were evaluated. For this purpose two techniques were employed, namely X-ray reflectivity (XRR) and X-ray diffraction (XRD) both at normal and grazing incidence angle. The samples were characterized before and after the irradiations.

The least square fit of the XRR data shows that the Fe layer for doses up to 27.6 dpa has an average atomic density similar to that of bulk Fe (8.5×10^{28} atoms/m^3). For higher doses two Fe sublayers (top and bottom sublayer), with about 100 nm thickness each, were found with different atomic densities. The correspondence of these two sublayers with the radiation damage and implantation induced by the Fe^+ ion irradiations is presented in Fig. 1. The top sublayer corresponds to the depth in which radiation damage is the main effect and the bottom sublayer relates to the depth in which both damage and implantation exist. The density of the top and bottom sublayers reaches the value of 8.9×10^{28} at/m^3 and 9.2×10^{28} at/m^3, respectively, for the maximum dose of 341 dpa.

The XRD measurements at normal and grazing incidence angle (GIXRD) reveal a bcc crystalline structure of the as fabricated Fe films. The crystallinity remains even after the irradiation of 341 dpa, whereas it is observed that as the dose increases the (110) Bragg peak moves to lower angles showing an increase of the lattice constant (Fig. 2). The lattice constant increases with the increase of the dose from 0.2859(7) nm for the un-irradiated sample to 0.2869(3) nm for the maximum dose of 341 dpa. A similar

Please cite this article as: K. Papamihail et al., Fe^+ ion irradiation induced changes in structural and magnetic properties of iron films, Nuclear Materials and Energy (2016), http://dx.doi.org/10.1016/j.nme.2016.03.006

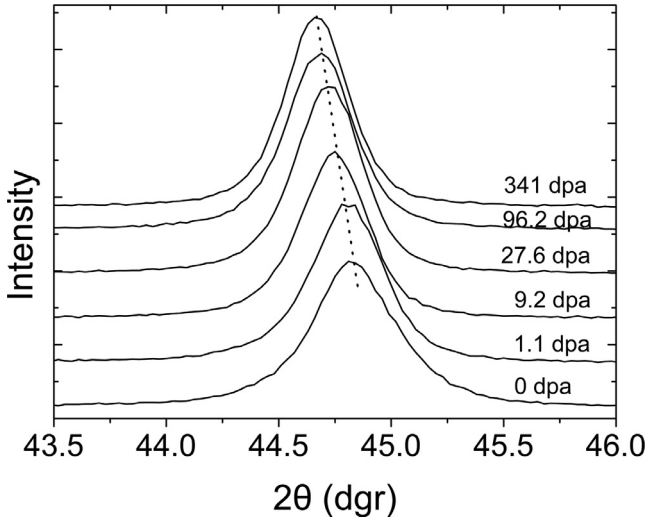

Fig. 2. The Fe (110) Bragg peak for various irradiation doses.

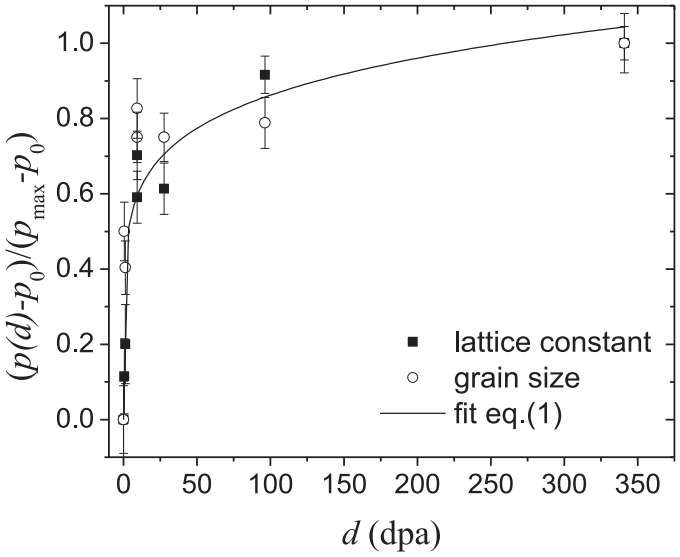

Fig. 3. Normalized lattice constant and grain size as a function of irradiation dose. Continuous line is least squares fit of Eq. (1) to the data (see 3.1 for details).

behavior was found in our previous work [7] regarding the irradiation effects of 490 keV Fe^+ ions on 60 nm thick Fe films. The lattice constant as measured by GIXRD, which corresponds to the out of plane lattice constant, coincides, within error bar, with the lattice constant measured with normal XRD using the (110) peak. In our previous work [7], where only recoils prevail and implantation effects are negligible, we observed a 25% decrease in the integrated intensity of the (110) Fe Bragg peak for the maximum dose of 70 dpa. In the current work no systematic variation of the (110) integrated intensity is found.

From peak profile analysis of the (110) XRD peak the mean grain size can be calculated [11]. The values of the grain size vary between 24 nm, for the non-irradiated sample, up to 31 nm for the highest dose of 341 dpa.

Both the lattice constant and the grain size increase monotonically with dose. One observes an initial stage where the lattice constant and the grain size increase abruptly and a second stage where both properties approach slowly the saturation. The variation of the lattice constant and the grain size versus dose, d, in dpa shows a common behavior that can be described by the equation

$$\left(\frac{p(d)-p_0}{p_{\max}-p_0}\right)^n = K\cdot d \qquad (1)$$

where p is the property in question (i.e. either lattice constant or grain size) and p_0 and $p_{\max}$ are the property values for zero and maximum dose, respectively (Fig. 3). The exponent n, as obtained from the least square fit of Eq. (1) to the data of both the lattice constant and grain size, is determined for both properties as 6.4±1.1 whereas the constant K has a value $(3.9\pm1.7)\times10^{-3}$ dpa^{-1}. The fitted curve is presented in Fig. 3 as a solid line together with the scaled according to Eq. (1) lattice constant and grain size.

Lattice constant increase was found in a previous study [12] of fission and 14 MeV neutron irradiation of Mo and it was attributed to the lattice strain from interstitials and small interstitial cluster. Gray and Cummings [13] found that the lattice constant of fission neutron irradiated Mo presents a maximum at some dose and at higher doses it decreases below the pre-irradiation value. The explanation of this behavior is based on the clustering and growth of the interstitial which presupposes the presence of a considerable number of interstitial traps such as impurities.

Ion irradiation has been observed to induce grain growth in thin polycrystalline metal film and it has been theoretically investigated in a number of studies [14–18 and references therein]. Grain growth by ion irradiation may be caused by increased atomic mobility, indirectly through mobile radiation induced crystal defects and directly through atomic collisions. The role of each mechanism in ion irradiation enhanced grain growth is still unclear. Alexander and Was [15] and Kaoumi and co-workers [16] proposed a thermal spike model to describe the grain growth. In some of these studies the grain growth follows the law $w^n - w_0^n = K\Phi$ where w_0 the grain size of the un-irradiated sample, K is proportional to the grain boundary mobility, Φ the ion dose and n a constant. The growth exponent was found to vary in the range 1.0–4.5. We observe that, in the current work, the power law is applicable for both the scaled lattice constant and grain size over the whole range of doses. However, in the current work the exponent n is found to be larger, i.e. 6.4±1.1.

3.2. Magnetic changes induced by Fe^+ irradiation

The induced magnetic state changes were determined by measuring the magnetic hysteresis loop for the various irradiation doses (Fig. 4). The saturation magnetization of the samples after the irradiation presents a non-monotonous variation. The magnetization increases up to about 16% for the dose of 96.2 dpa, whereas at the much larger dose of 341 dpa it is reduced to a value 7% larger than that in the non-irradiated state, as it can be seen in Fig. 4. These results will be discussed below in conjunction with the PNR measurements.

One observes a drastic decrease in the coercive field, H_c, with the increase of the dose from 85 Oe for the un-irradiated samples to 17 Oe for the sample irradiated at 341 dpa (see inset of Fig. 4). In Fig. 5 is presented the coercive field as a function of the inverse grain size. The graph of H_c versus the inverse of the grain size shows two linear regions with slopes 2±1 Oe·μm and 12.1±2.6 Oe·μm corresponding to the low and high doses, respectively. In our previous work [7], where doses up to about 70 dpa were investigated, the slope was found 3.18±0.13 Oe•μm which is in closer agreement with the first slope that corresponds to low doses. Yensen and Ziegler [19] have found in bulk iron that the grain boundary contribution in the coercivity is $H_c(Oe) = 3.7\times10^{-3}/L(\text{cm})$ where L is the mean grain diameter. For our nanocrystalline films this contribution is one order of magnitude smaller. Kamada et al. [20,21] found that in monocrystalline 30 and 250 nm thick Fe films the magnetic hysteresis curves are not influenced by

Please cite this article as: K. Papamihail et al., Fe^+ ion irradiation induced changes in structural and magnetic properties of iron films, Nuclear Materials and Energy (2016), http://dx.doi.org/10.1016/j.nme.2016.03.006

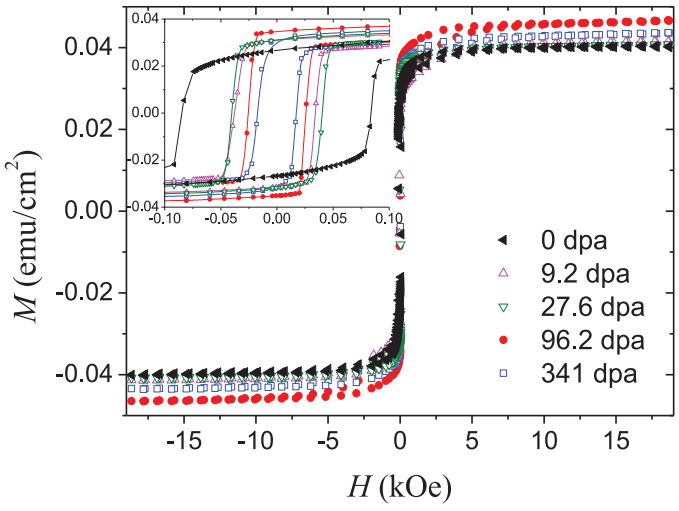

Fig. 4. Magnetization hysteresis curves for various irradiation doses. The inset shows a magnification of the hysteresis curve around zero field.

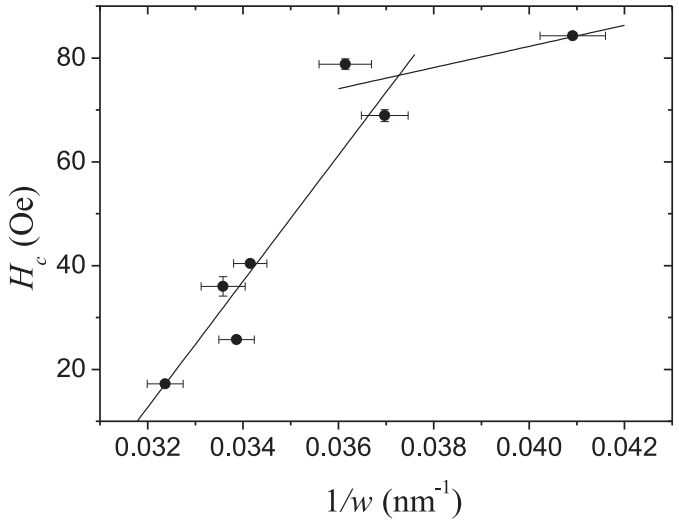

Fig. 5. The coercive field as a function of inverse grain size. The lines are least square fits (see 3.2 for details).

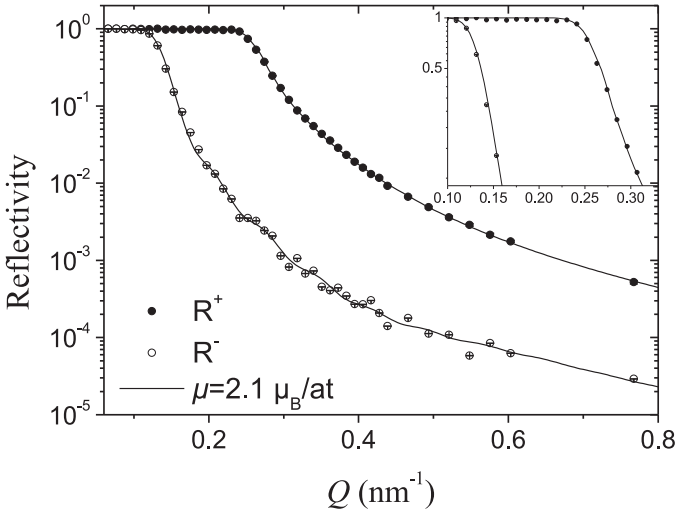

Fig. 6. PNR data of the non-irradiated sample. The solid line is a least-square fit to the data. The inset shows the spin up and down reflectivity near the critical region.

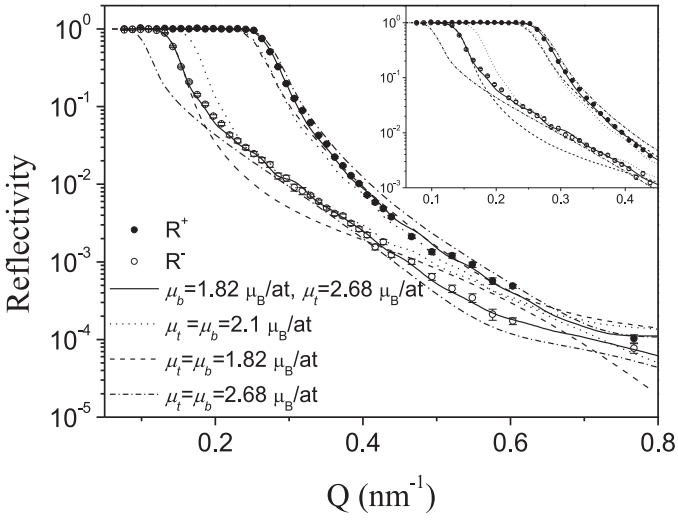

Fig. 7. PNR data of sample irradiated at 96.2 dpa. The solid line is a least-square fit to the data with μ_b=1.82 μ_B/at and μ_t=2.68 μ_B/at. The dotted, dashed and dashed-dotted lines correspond to models with μ_t=μ_b=2.1 μ_B/at, μ_t=μ_b=1.82 μ_B/at and μ_t=μ_b=2.68 μ_B/at, respectively (see 3.2 for further explanation). The inset shows the spin up and down reflectivity near the critical region.

the irradiation of 3.2 MeV Ni^+ ions up to a fluence of 6.4×10^{14} ions/cm^2. This different behavior compared to our findings must be due to the fact that in the current study three orders of magnitude higher doses are used.

In order to resolve whether there is a magnetization profile associated with the enhanced magnetization observed in the magnetic hysteresis loop PNR measurements were employed. For the fitting of the PNR data both a structural and a magnetic model have to be incorporated in the least squares fitting. In order to reduce the number of parameters to be fitted by the least squares procedure the structural parameters determined by XRR formed the basis for the structural models used for the interpretation of the PNR spectra. The atomic density and thickness parameters of the profile (which was simulated using two main Fe sublayers) were used in the initial model for the least fit of the PNR data in order to deduce the magnetic moment profile.

The PNR data of the un-irradiated sample are depicted in Fig. 6. The spin up and spin down reflectivities are presented with their least-square fitted curves (solid line curves). The Fe magnetic moment is determined to be equal to 2.10±0.05 μ_B/atom. This value is about 3.7% lower than that expected for the bulk Fe at room temperature calculated from its magnetization versus temperature curve [22]. From the magnetic hysteresis loop (Fig. 4) we observe that the magnetic field used for the PNR measurements of 1.2 T results in a magnetization of around 1% lower than the saturation value. Thus the by PNR found lower value than the bulk one of the Fe film magnetic moment arises from the lack of complete saturation. Taking this into account and recalculating the expected magnetic moment in the applied filed of 1.2 T it is found that the value of the magnetic moment in the un-irradiated 200 nm Fe film determined by PNR agrees extremely well with the value of bulk iron at room temperature.

The spin up and spin down reflectivities for the sample irradiated at 96.2 dpa are shown in Fig. 7. In order to fit the experimental PNR data one has to assume a magnetic depth profile consisting of two sublayers the top one with thickness and magnetic moment per atom h_t and μ_t, respectively and the bottom one having the values h_b and μ_b. From a least squares fit to both reflectivities (continuous line in Fig. 7) the magnetic moments of the two sublayers of the Fe film irradiated at 96.2 dpa were determined to be

Please cite this article as: K. Papamihail et al., Fe^+ ion irradiation induced changes in structural and magnetic properties of iron films, Nuclear Materials and Energy (2016), http://dx.doi.org/10.1016/j.nme.2016.03.006

μ_t=2.68 μ_B/atom (h_t=120 nm) and μ_b=1.82 μ_B/atom (h_b=80 nm), respectively. It should be reminded that these two sublayers were found by XRR measurements to have different atomic densities and should be correlated with the Fig. 1, with the top sublayer corresponding to the region in which we have mostly displacement of the atoms and the bottom sublayer where implantation prevails. In order to show the accuracy of the magnetic moment determination two simulations with μ_t=μ_b=2.68 μ_B/atom and μ_t=μ_b=1.82 μ_B/atom magnetic moment values are shown in Fig. 7. Further in Fig. 7 we show the calculated PNR curve for Fe magnetic moment of 2.1 μ_B/atom, the value found for the un-irradiated sample. Comparison of this with the experimental data leaves no doubt about the sensitivity of the PNR technique in determining the magnetic profile and the accuracy of the deduced magnetic moments for which the error is estimated to be around 2.5%. In this stage some aspects of the PNR techniques have to be brought to the reader's attention. PNR is very sensitive in determining magnetic or density variations versus depth but it averages over the *xy* plane. Thus, the determined magnetic moment is an average over the Fe sublayer volume. This means that either all the atoms have the determined magnetic moment value or there are regions of higher and lower magnetic moments per atom dispersed randomly over the whole volume of the sublayer and the mean obtained by averaging over all regions equals to the determined value.

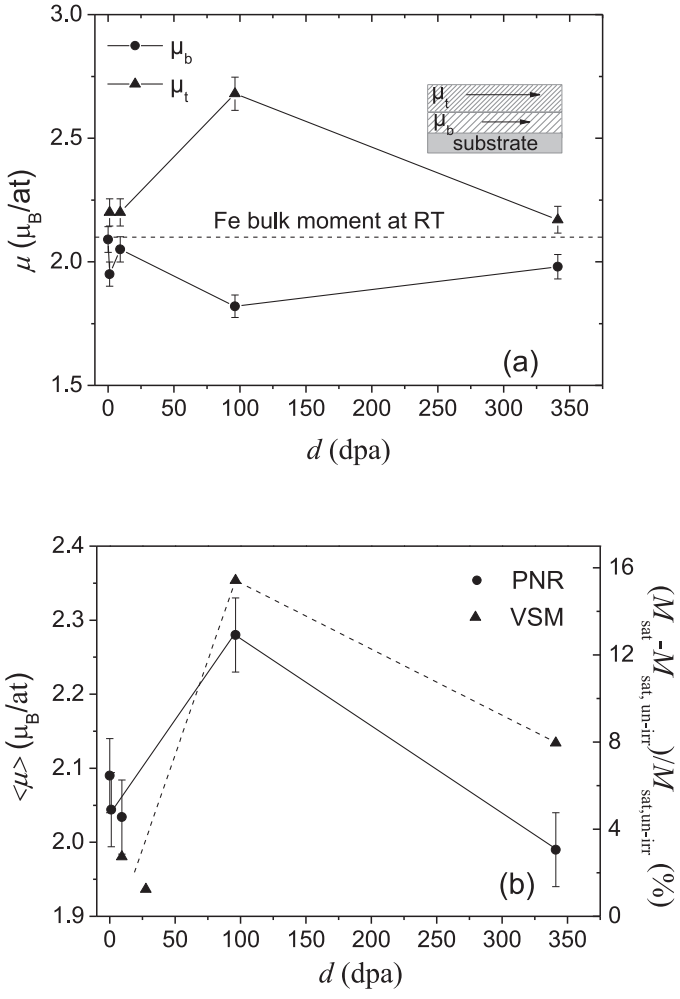

Fig. 8. (a) Atomic magnetic moment for the two Fe sublayers as a function of dose. (b) Average magnetic moment as determined from PNR data as a function of dose (■) and the % variation of the saturation magnetization with respect to that of the un-irradiated sample (▲). The solid lines are guide to the eye.

The variation of the atomic magnetic moment, μ, as determined by PNR for the two Fe sublayers versus ion dose in dpa, *d*, is depicted in Fig. 8a. It is observed that the magnetic moment for the top Fe sublayer presents a maximum at the dose of 96.2 dpa and for higher doses it decreases towards the Fe bulk moment at room temperature. The magnetic moment of the bottom Fe sublayer presents small variation as a function of dose and it shows a minimum of 1.82 μ_B/atom also at the dose of 96.2 dpa. This behavior versus dose is in agreement with variation of the saturation magnetization as measured by the magnetic hysteresis loop (Fig. 8b). It is pointed out that the magnetic depth dependent profile, presented in Fig. 8, is not related to Cr diffusion in the Fe layer, since elemental mapping (not shown in the present work) of the cross section of the film irradiated at the highest dose, by TEM measurements, show Cr only on the surface. Further, it is noted that the analysis of the PNR data reveals the presence of a chromium oxide film on the surface having a thickness of about 3–4 nm.

4. Discussion and conclusions

The 490 keV self-ion irradiation of 200 nm Fe films was found to induce both structural and magnetic changes. The bcc crystal structure remains even after a dose of 341 dpa. By XRR measurements it has been found that for doses larger than 27.6 dpa two density sublayers have been formed. Lattice expansion and grain growth are observed. Their increase versus irradiation dose follows the same growth equation (Eq. 1). This correlation of grain size and lattice constant increase versus defect production (dpa) is an important finding which demonstrates that any models of radiation damage should aim in explaining not only the alteration of physical properties arising from the irradiation but also the correlation of the induced changes as that depicted in Fig. 3.

The analysis of the PNR data of the irradiated samples shows a magnetic depth profile with the top Fe sublayer having an enhanced magnetic moment whereas the bottom Fe sublayer exhibits a reduction of the magnetic moment. In addition the magnetic moment of both layers varies as a function of irradiation dose as depicted in Fig. 8a. The enhancement of the magnetic moment of the top Fe sublayer is in agreement with that found in our previous work [7] for Fe film thickness of 60 nm. In this latter case only recoils take place, whereas implantation effects are negligible. However, in 200 nm thick Fe films implantation effects start to play a role for depths larger than about 80 nm (Fig. 1).

Having shown the enhancement of the Fe magnetic moment for films having a thickness of 60 nm [7], we attribute the magnetic moment increase/decrease to an atomic volume increase/decrease. The increase of the magnetic moment with increasing atomic volumes has been shown by ab initio calculations [23,24]. Using the empirical formula [25] $\mu = \mu_C(1-\sqrt{v_c/v})^\gamma$ (v is the atomic volume and v_c a critical atomic volume corresponding to the onset of ferromagnetism), the observed magnetic moment of 2.68 μ_B/atom after the 96.2 dpa irradiation corresponds to an atomic volume of 18.45 Å^3. A lattice expansion after irradiation has been observed in the current study, however the atomic volume that corresponds to the 96.2 dpa is merely 11.8 Å^3, close to that of bulk iron. Intuitively we may imagine that a rich of vacancies region which increases the average atomic volume would have the same result. A concentration of vacancies around 36% would give a mean atomic volume of 18.45 Å^3 and thus an average magnetic moment per Fe atom of 2.68 μ_B. It has been found by atomistic computer simulations in α-Fe that 2NN and 3NN vacancy dimers (the second and the third nearest neighbor sites) are stable energetically and larger vacancy clusters can be formed by combinations of the triangular trimers and the square tetramers on {100} plane [26]. Also from kinetic Monte Carlo it was found that vacancy clusters are mobile having

Please cite this article as: K. Papamihail et al., Fe$^+$ ion irradiation induced changes in structural and magnetic properties of iron films, Nuclear Materials and Energy (2016), http://dx.doi.org/10.1016/j.nme.2016.03.006

increasing with the size energy for migration and dissociation [27]. Therefore, it is plausible to assume that the increase of the magnetic moment observed arises from the presence of vacancy clusters. These vacancy clusters would have as an effect the reduction of the local electronic density, ρ. Correlating the magnetic moment with the electronic density described by a simple model [28] we find that reduction of the relative electronic density ρ/ρ_c (ρ_c a density corresponding to the onset of ferromagnetism) from 0.84 to 0.71 corresponds to an increase of the magnetic moment from 2.1 to 2.68 μ_B/atom. Following the same reasoning for the decrease of magnetic moment of the bottom Fe sublayer we find that the decrease to 1.82 μ_B/atom for the dose of 96.2 dpa corresponds to a reduction of the atomic volume to 10.6 Å^3 which might be attributed to a concentration of interstitials of 11%. However, the percentage of the implanted Fe atoms is much lower, of about 1.4% at this dose. We might speculate that compressive stresses due to interstitials decrease the average atomic volume resulting to the lower magnetic moment observed.

Above we have offered a plausible explanation of the magnetic profile induced in Fe films by the 490 keV Fe^+ ion irradiation. However, further experiments and calculations are needed in order to elucidate the current experimental findings and to resolve the type and density of defect complexes, e.g. vacancy and/or interstitial clusters, which remain after an irradiation with 490 keV Fe^+.

Acknowledgments

The authors would like to thank Dr M. Gjokas and Prof. I. Panagiotopoulos for their help in the magnetization measurements, as well as the Physics Department of the University of Ioannina for the provision of the magnetometer. This work has been carried out within the framework of the EUROfusion Consortium and has received funding from the Euratom research and training programme 2014—2018 under grant agreement number No 633053. The experiment at LLB was supported by the European Commission through the Access Activities of the Integrated Infrastructure Initiative for Neutron Scattering and Muon Spectroscopy (NMI3), supported by the European Commission under the 7th Framework Programme through the Key Action: Strengthening the European Research Area, Research Infrastructures, Contract NMI3-II/FP7 No. 283883. The views and opinions expressed herein do not necessarily reflect those of the European Commission.

References

[1] R. Lässer, N. Baluc, J.-L. Boutard, E. Diegele, S. Dudarev, M. Gasparotto, A. Möslang, R. Pippan, B. Riccardi, B. van der Schaaf, Fusion Eng. Des. 82 (2007) 511–520.
[2] StevenJ. Zinkle, NasrM. Ghoniem, J. Nucl. Mater. 417 (2011) 2–8.
[3] M. Gasparotto, R. Andreani, L.V. Boccaccini, A. Cardella, G. Federici, L. Giancarli, G. Le Marois, D. Maisonnier, S. Malang, A. Möslang, Y. Poitevin, B. van der Schaaf, M. Victoria, Fusion Eng. Des. 66–68 (2003) 129–137.
[4] Derek Stork, Pietro Agostini, Jean-Louis Boutard, Derek Buckthorpe, Eberhard Diegele, SergeiL. Dudarev, Colin English, Gianfranco Federici, MarkR. Gilbert, Sehila Gonzalez, Angel Ibarra, Christian Linsmeier, Antonella Li Puma, Gabriel Marbach, LeeW. Packer, Baldev Raj, Michael Rieth, MinQuang Tran, DavidJ. Ward, StevenJ. Zinkle, Fusion Eng. Des. 89 (2014) 1586–1594.
[5] S.J. Zinkle, J.P. Blanchard, R.W. Callis, C.E. Kessel, R.J. Kurtz, P.J. Lee, K. McCarthy, N.B. Morley, F. Najmabadi, R.E. Nygren, G.R. Tynan, D.G. Whyte, R.S. Willms, B.D. Wirth, Fusion Eng. Des. 89 (2014) 1579–1585.
[6] G.S. Was, R.S. Averback, Comprehensive Nuclear Materials, Vol. 1.07, Elsevier, 2012, p. 195.
[7] K. Papamihail, K. Mergia, F. Ott, Yves Serruys, Th. Speliotis, G. Apostolopoulos and S. Messoloras, Phys. Rev. B **93**, 2016, 100404-1-5.
[8] J.F. Ziegler, J.P. Biersack, U. Littmark, The Stopping and Range of Ions in Solids, Pergamon, New York, 1985 (SRIM-2008 code: http://www.srim.org/).
[9] ASTM Standard E693-94, Standard practice for characterising neutron exposure in iron and low alloy steels in terms of displacements per atom (dpa), 1994.
[10] http://www-llb.cea.fr/prism/programs/simulreflec/simulreflec.html, version 1.9.
[11] Mario Birkholz, Thin Film Analysis by X-ray Scattering, WILEY-CVH Verlag GmbH & Co., KGaA, Weinheim, 2006, pp. 108–115.
[12] J.L. Brimhall, L.A. Charlot, H.E. Kissinger, Radiat. Eff. 28 (1976) 115–117.
[13] D.L. Gray, W.V. Cummings, Acta Met 8 (1960) 446–452.
[14] D. Kaoumi, A.T. Motta, R.C. Birtcher, J. ASTM Int. 4 (2007) 1–13.
[15] D.E. Alexander, G.S. Was, Phy. Rev. B 47 (1997) 2983–2994.
[16] D. Kaoumi, A.T. Motta, R.C. Birtcher, J. Appl. Phys. 104 (2008) 1–13.
[17] J.C. Liu, J.W. Mayer, J Nucl. Instrum. Methods B 20 (1987) 538–542.
[18] N. Karpe, J. Bottiger, N.G. Chechenin, J.P. Krog, Mater. Sci. Eng. 180 (1994) 582–586.
[19] T.D. Yensen, N.A. Ziegler, Trans. Am. Soc. Metals 23 (1935) 556.
[20] Y. Kamada, H. Watanabe, S. Mitani, J. Echigoya, H. Kikuchi, S. Kobayashi, N. Yoshida, Koki Takanashi, Mater. Trans. 50 (2009) 2134–2138.
[21] Y. Kamada, H. Watanabe, S. Mitani, J. Echigoya, J.N. Mohapatra, H. Kikuchi, S. Kobayashi, K. Takanashi, J. Phys.: Conf. Ser. 266 (2011) 1–5.
[22] Soshin Chikazumi, Physics of Magnetism, John Wiley & Sons, Inc., New York, 1964.
[23] H.C. Herper, E. Hoffmann, P. Entel, Phys. Rev. B 60 (1999) 3839–3848.
[24] M. Černý, J. Pokluda, M. Šob, M. Friák, P. Šandera, Phys. Rev. B 67 (035116) (2003) 1–8.
[25] P.M. Derlet, S.L. Dudarev, Prog. Mater. Sci. 52 (2007) 299–318.
[26] F. Ye, C. Yin, K. Tong, C. Zhang, W.B. Liu, Mater. Res. Innov. 18 (S4) (2014) 1003–1006.
[27] F.G. Djurabekova, L. Malerba, C. Domain, C.S. Becquart, Nucl. Instrum. Methods B 255 (2007) 47–51.
[28] S.L. Dudarev, P.M. Derlet, J. Comput. Aided Mater. Des. 14 (2007) 129–140.

Please cite this article as: K. Papamihail et al., Fe^+ ion irradiation induced changes in structural and magnetic properties of iron films, Nuclear Materials and Energy (2016), http://dx.doi.org/10.1016/j.nme.2016.03.006